IOPscience iopscience.iop.org

Home Search Collections Journals About Contact us My IOPscience

Lanthanide 4f-level location in $AVO_4:Ln^{3+}$ (A = La, Gd, Lu) crystals

This article has been downloaded from IOPscience. Please scroll down to see the full text article.

2009 J. Phys.: Condens. Matter 21 115503

(http://iopscience.iop.org/0953-8984/21/11/115503)

View the table of contents for this issue, or go to the journal homepage for more

Download details:
IP Address: 129.252.86.83
The article was downloaded on 29/05/2010 at 18:38

Please note that terms and conditions apply.

J. Phys.: Condens. Matter **21** (2009) 115503 (8pp) doi:10.1088/0953-8984/21/11/115503

Lanthanide 4f-level location in $AVO_4:Ln^{3+}$ (A = La, Gd, Lu) crystals

Andreas H Krumpel[1,6], Erik van der Kolk[1], Enrico Cavalli[2], Philippe Boutinaud[3], Marco Bettinelli[4,5] and Pieter Dorenbos[1]

[1] Faculty of Applied Sciences, Delft University of Technology, Mekelweg 15, 2629 JB Delft, The Netherlands
[2] Dipartimento di Chimica Generale ed Inorganica, Chimica Analitica, Chimica Fisica, Università di Parma, Parma, Italy
[3] Laboratoire des Matériaux Inorganiques—UMR 6002, Université Blaise-Pascal et ENSCCF, Aubière, France
[4] Dipartimento Scientifico e Tecnologico, Università di Verona, Verona, Italy
[5] INSTM, UdR Verona, Ca' Vignal, Strada Le Grazie 15, 37134 Verona, Italy

E-mail: a.h.krumpel@tudelft.nl

Received 23 December 2008
Published 20 February 2009
Online at stacks.iop.org/JPhysCM/21/115503

Abstract

The spectral properties of $LaVO_4$, $GdVO_4$ and $LuVO_4$ crystals doped with Ce^{3+}, Pr^{3+}, Eu^{3+} or Tb^{3+} have been investigated in order to determine the position of the energy levels relative to the valence and conduction bands of the hosts along the trivalent and divalent lanthanide series. Pr^{3+} and Tb^{3+} ground state levels are positioned based on the electron transfer energy from those states to the conduction band, the so-called intervalence charge transfer (IVCT). This approach is compared with an alternative model that is based on electron transfer from the valence band to a lanthanide.

(Some figures in this article are in colour only in the electronic version)

1. Introduction

Many lanthanide (Ln = La, Ce, . . . , Lu) doped orthovanadates of rare earth metals ($REVO_4:Ln^{3+}$; RE = rare earth) are well known compounds for different applications such as laser host crystals or phosphor materials. Their luminescence properties depend strongly on the location of the 4f energy levels of the Ln dopants relative to the valence band (VB) and the conduction band (CB) of the host. Following up a previous work on $LaVO_4:Ln^{3+}$ [1], we have recorded temperature-dependent photoluminescence emission and excitation spectra of $GdVO_4:Ln^{3+}$ and $LuVO_4:Ln^{3+}$ (Ln = Ce, Pr, Eu, Tb) crystals. The objective of this study was to construct energy level diagrams for the Ln doped orthovanadates of gadolinium and lutetium explaining the dependence of the luminescence properties on the Ln dopants for each host. Boutinaud *et al* identified in $GdVO_4:Pr^{3+}$ and $LuVO_4:Pr^{3+}$ the 'virtual recharge' mechanism or intervalence charge transfer (IVCT), i.e. an electron transfer from Pr^{3+} to the VO_4^{3-} group [2]. The IVCT model of Boutinaud shows a linear correlation between the IVCT energy and the optical electronegativity of the transition metal cation divided by the shortest distance between the Ln dopant and the cation (here V^{5+}) to be reduced. The proposed mechanism provides information on the 4f ground state (GS) energy of the trivalent Ln dopant ions relative to the VB and the CB and hence it is complementary to the Dorenbos model. This latter model relies on the observation that the energy difference between the Ln 4f ground state (GS) energy and the top of the VB reveals independently from the host a characteristic zig-zag shape when the number of electrons in the 4f shell increases from 1 (Ce^{3+}, La^{2+}) to 14 (Lu^{3+}, Yb^{2+}) [3]. This means that knowledge of the absolute 4f GS energy location of only one Ln dopant ion, that is its location relative to the CB and the VB of the host matrix, suffices to predict the absolute 4f GS energy locations of all the other possible Ln dopants. The CT energies as well as the temperature quenching behavior of some of the excitation and emission bands can provide indispensable information about the 4f GS energies of the Ln dopant ions relative to the electronic host states.

[6] Author to whom any correspondence should be addressed.

 © 2009 IOP Publishing Ltd Printed in the UK

Table 1. r = effective ionic radius [9]; SG = space group [18, 22]; PG = point group symmetry (Schoenflies); χ_P = electronegativity (Pauling scale); $\langle d(\text{R–O})\rangle$ (R = A, V) = average interatomic distance in polyhedra of the AVO_4 structure [18, 22].

AVO_4	r(A) (pm)	χ_P(A)	SG (Nr.)	$\langle d(\text{A–O})\rangle$ (pm)	$\langle d(\text{V–O})\rangle$ (pm)	PG
$LaVO_4$	121.6	1.1	$P2_1/n$ (14)	259.7	170.9	C_{2h}
$GdVO_4$	105.3	1.2	$I4_1/amd$ (141)	248.3	160.4	D_{2d}
YVO_4	101.9	1.22	$I4_1/amd$ (141)	236.5	170.88	D_{2d}
$LuVO_4$	97.7	1.27	$I4_1/amd$ (141)	233.1	170.67	D_{2d}

2. Experimental details

2.1. Sample preparation

All crystals were prepared by the flux growth method using $Pb_2V_2O_7$ as the solvent. Pure Lu_2O_3, Gd_2O_3, V_2O_5, PbO and $Na_2B_4O_7$ were used as starting materials [4]. The composition of the growth mixtures was (in molar per cent ratio): Lu_2O_3 (or Gd_2O_3):V_2O_5:PbO:$Na_2B_4O_7$ = 2.3:31.5:62.9:3.3. The dopants were added as Eu_2O_3, CeO_2, Tb_4O_7 or Pr_6O_{11} with a Ln/Lu(Gd) = 1% nominal molar ratio. After careful mixing, the starting mixtures were put in Pt crucibles and heated to 1270 °C in a horizontal programmable furnace. They were maintained at this temperature for 12 h (soaking time), then cooled to 800 °C at a rate of 1.8 °C and finally to room temperature at a rate of 15 °C. Transparent crystals in the form of platelets having an average size of 0.5 × 2 × 2 mm^3 were separated from the flux by dissolving it in hot diluted HNO_3.

$GdVO_4$ and $LuVO_4$ have the tetragonal zircon-type structure of YVO_4, with space group $I4_1/amd$ (Nr. 141). The Ln^{3+} ions are eight-fold coordinated by oxygen forming dodecahedral cages having D_{2d} point symmetry, whereas the V^{5+} ions are tetrahedrally coordinated by oxygen atoms [5–7]. The main differences between the two matrices are related to the presence of two cations, Lu^{3+} and Gd^{3+}, having different ionic radii and electronegativities, as summarized in table 1. Despite the similarities of the structural properties and the same site symmetry, the luminescence properties of an activator can significantly differ on passing from one member of the $LnVO_4$ family to another. The $^5D_4 \rightarrow {}^7F_J$ luminescence of Tb^{3+}, for instance, can be observed in $GdVO_4$ and $LuVO_4$ but shows no emission at all in YVO_4 [8]. The effective ionic radii, r, of these rare earth elements with coordination number 8 increases as follows: $r(Gd^{3+}) > r(Y^{3+}) > r(Lu^{3+})$ [9]. Hence, the absence of Tb^{3+} luminescence in YVO_4 cannot be explained simply by the size of Y^{3+} or by the symmetry of the coordination polyhedra.

2.2. Measurement techniques

A 450 W xenon lamp (FL-1039) was used in combination with a double-grating monochromator (Gemini-180, Horiba J Y, USA) as an excitation source. The light emitted from the crystals was detected by a single photon counting module with a channel photomultiplier (CPM, model MP-1993, PerkinElmer) after traversing a 100 mm focal length monochromator (model MCG 910, Macam Photometrics Ltd). Excitation spectra were corrected for background and lamp spectrum (obtained with a calibrated SXUV-type Si-ultraviolet photodiode from IRD) whereas the emission spectra where corrected for the background and the transmission of the Macam monochromator in combination with the CPM. Low temperatures (down to 8 K) were achieved with a SHI-APD helium compressor (model HC-4) connected to a two-stage cryogenic refrigerator (model DE204); temperature control was achieved with a temperature controller (model 331, Lake Shore Cryotronics, Inc.).

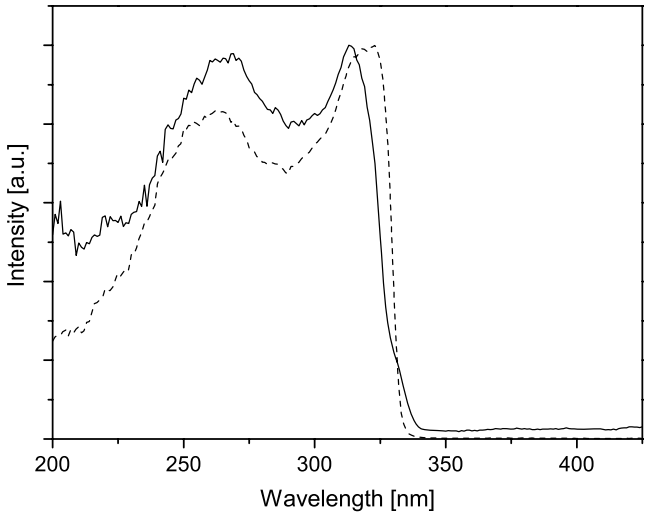

Figure 1. Normalized excitation spectra at 15 K of $GdVO_4$:1%Ce^{3+} (solid line) and $LuVO_4$:1%Ce^{3+} (dashed line) monitoring the emission at 447 nm.

3. Results

3.1. $GdVO_4$:1%Ce^{3+} and $LuVO_4$:1%Ce^{3+}

The Ce^{3+} ion is known to be non-luminescent in vanadate lattices. Figure 1 shows the excitation spectra of $GdVO_4$:Ce^{3+} and $LuVO_4$:Ce^{3+} at 15 K monitoring the host emission at 447 nm. This spectrum is consistent with that reported and discussed by Ronde and Blasse for YVO_4 [10]. Accordingly, we assign the band at 250 nm to the $^1A_1 \rightarrow {}^1T_2(t_1 \rightarrow e)$ (symmetry allowed) and the band at 310–320 nm to the $^1A_1 \rightarrow {}^1T_1(t_1 \rightarrow e)$ (symmetry forbidden) absorption transition of the VO_4^{3-} ion. In figure 2 the 15 K emission spectra of $GdVO_4$:Ce^{3+} and $LuVO_4$:Ce^{3+} are presented. They show the typical VO_4^{3-} group emission band with maxima at 436 nm ($GdVO_4$:Ce^{3+}) and 444 nm ($LuVO_4$:Ce^{3+}) which is assigned to the $^3T_1 \rightarrow {}^1A_1$ transition [11, 12]. The weak features in the long wavelength tail of the emission band can presumably be ascribed to unwanted impurities [13].

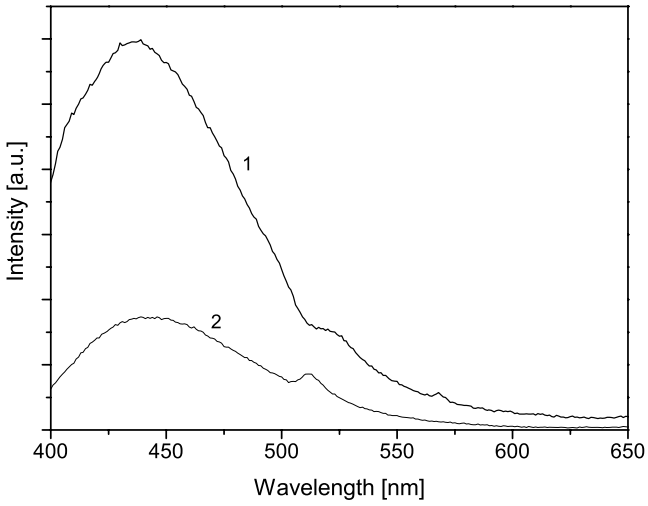

Figure 2. Emission spectra of $GdVO_4$:1%Ce^{3+} (curve 1) and $LuVO_4$:1%Ce^{3+} (curve 2); the spectra were recorded at 15 K under 312 nm excitation.

3.2. *$GdVO_4$:0.6%Pr^{3+} and $LuVO_4$:0.2%Pr^{3+}*

The optical properties of Pr^{3+} in gadolinium and lutetium orthovanadates were investigated at room temperature in a previous study [2]. The 15 and 200 K excitation spectra of $GdVO_4$:Pr^{3+} and $LuVO_4$:Pr^{3+} monitoring the $^3P_0 \rightarrow {}^3H_6$ (625 nm) emission are shown in figure 3. In $GdVO_4$:Pr^{3+} (figure 3(a)) three UV bands can be noticed: at 250 nm, 310–320 nm and 383 nm, respectively. The two former are due to transitions within the VO_4^{3-} complex as found in AVO_4:Ce^{3+} (A = Gd, Lu). The latter band at 383 nm is ascribed to the IVCT. This position differs by some 20 nm from a value previously reported at room temperature for a crystal doped with a smaller amount of Pr^{3+} [2]. It is not the purpose of the present work to study a possible Pr^{3+} concentration effect on the IVCT position, but it has to be noticed than in [2] the IVCT band appeared only as a shoulder in the excitation spectrum and was less accurately positioned than in the present investigation. At lower energies the $^3H_4 \rightarrow {}^3I_6, {}^3P_J$ excitation group (439–497 nm) can be seen. $LuVO_4$:Pr^{3+} (figure 3(b)) shows beside the VO_4^{3-} group and $^3H_4 \rightarrow {}^3P_J$ multiplet transitions a broad band between 360–440 nm which is composed of at least two different bands with different temperature behaviors. Boutinaud *et al* have identified the IVCT in $LuVO_4$:Pr^{3+} at about 396 nm [2]. This is in agreement with the low excitation band at 200 K. At 15 K though the IVCT band is overlapped by a broad band (hereafter referred to as the U transition) peaking at 418 nm.

Figure 4 shows the emission spectra of $GdVO_4$:Pr^{3+} and $LuVO_4$:Pr^{3+} under $^3H_4 \rightarrow {}^3P_1$ (480 nm) excitation at 15 and at 200 K. The four prominent groups of emission are due to $^3P_0 \rightarrow {}^3H_5$ (544 nm), $^3P_0 \rightarrow {}^3H_6$ (625–644 nm), and $^3P_0 \rightarrow {}^3F_2$ (667 nm) transitions, similar to the ones identified in $YNbO_4$:Pr^{3+} [14, 15]. In the 200 K spectra an additional red band is present, assigned to the $^1D_2 \rightarrow {}^3H_4$ (615 nm) transition. In the adopted experimental conditions, in fact, the $^1D_2$ level can be populated by multi-phonon relaxation from

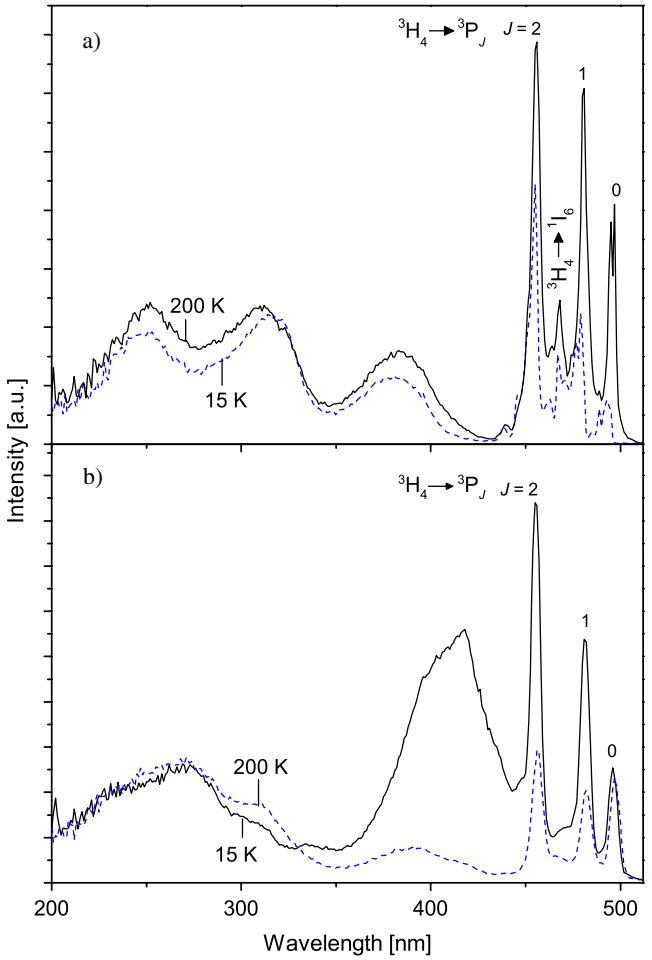

Figure 3. Excitation spectra of (a) $GdVO_4$:0.6%Pr^{3+} and (b) $LuVO_4$:0.2%Pr^{3+}; in all spectra the 625 nm emission was monitored.

the $^3P_0$ level or by radiationless relaxation through the IVCT state, thermally populated from $^3P_0$. At 15 K, both processes are inefficient and the emission arises from the $^3P_0$ level only. As the temperature increases, the $^1D_2$ population progressively increases as well as the intensity of the corresponding red emission. It has to be noted that the low temperature spectrum of Pr^{3+} in $LuVO_4$ overlaps a weak broadband with maximum at around 600 nm, probably associated with the weak U excitation band. The insets of figures 4(a) and (b) show the temperature quenching behavior of the $^3P_0 \rightarrow {}^3H_6$ (625 nm) emission under $^3H_4 \rightarrow {}^3P_1$ (483 nm) excitation.

3.3. *$GdVO_4$:1%Eu^{3+} and $LuVO_4$:1%Eu^{3+}*

Figure 5 shows the excitation spectra of $GdVO_4$:Eu^{3+} and $LuVO_4$:Eu^{3+} monitoring the $^5D_0 \rightarrow {}^7F_2$ (622 nm) emission at two different temperatures. Beside the $^7F_0 \rightarrow {}^5D_J$ multiplet transitions of Eu^{3+} two bands at 250 and at about 320 nm can be seen. These two bands are present in all excitation spectra presented in this work and have the same temperature behavior. As such, we assigned them to a VO_4^{3-} group transition. Liu *et al*, in contrast, ascribed the 250 nm band in $GdVO_4$:Eu^{3+} to the Eu^{3+} CT [16]. In the

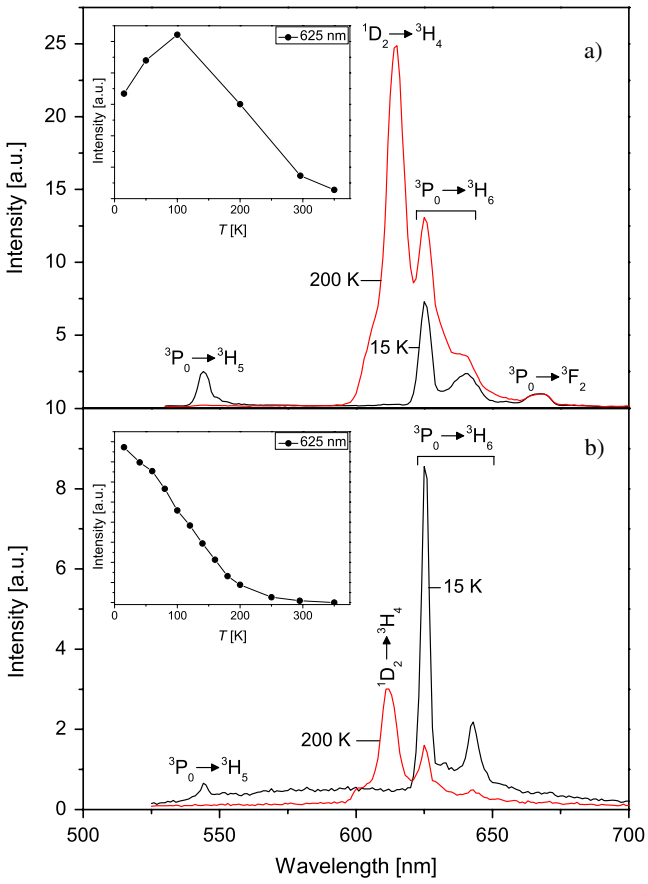

Figure 4. Emission spectra of (a) $GdVO_4$:0.6%Pr^{3+}, Exc = 480 nm and (b) $LuVO_4$:0.2%Pr^{3+}, Exc = 483 nm.

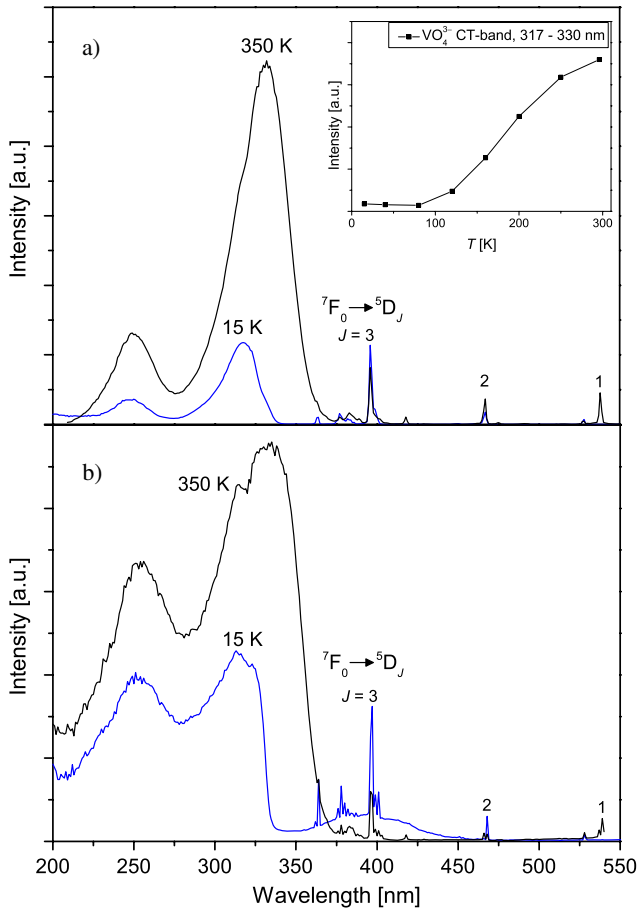

Figure 5. Excitation spectra of (a) $GdVO_4$:1%Eu^{3+} and (b) $LuVO_4$:1%Eu^{3+}; in all spectra the emission at 622 nm was monitored.

low temperature spectrum of $LuVO_4$:Eu^{3+} the U excitation band appears at around 394 nm. In both compounds the luminescence intensity increases with increasing temperature (see inset of figure 5(a)). The temperature behavior of the intensity of the main excitation band around 320 nm is consistent with the character of the involved $^1A_1 \rightarrow {}^1T_1$ transition: forbidden in T_d symmetry, it takes allowance from the static and dynamic (then thermally activated) distortions from the perfect tetrahedral geometry through the mixing of the low symmetry components of the $^1T_1$ and $^1T_2$ states [10].

In figure 6 the emission spectra of $GdVO_4$:Eu^{3+} and $LuVO_4$:Eu^{3+} are presented showing the typical $^5D_0 \rightarrow {}^7F_J$ multiplet emission peaks of Eu^{3+} [16]. In addition, both spectra present some barely observable features below 578 nm that can be ascribed to transitions from the $^5D_1$ level [17]. These are much more intense in the spectrum of $LuVO_4$:Eu^{3+} in which they overlap a broad band between about 500 and 700 nm which could relate to the low energy U excitation band at about 394 nm.

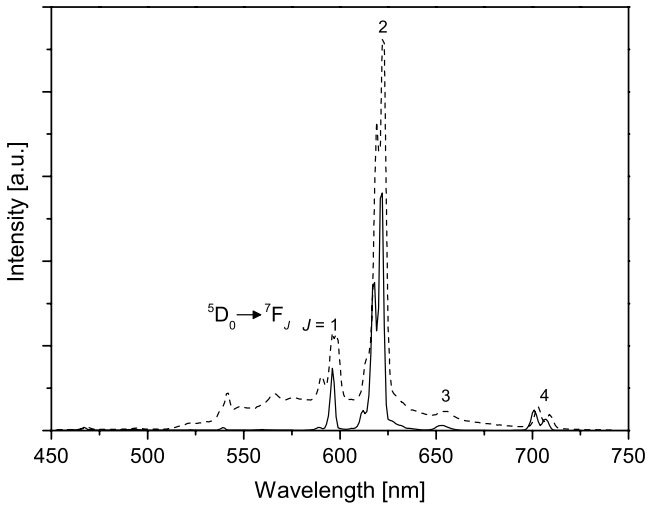

Figure 6. Emission spectra of $GdVO_4$:1%Eu^{3+} (solid curve) and $LuVO_4$:1%Eu^{3+} (dashed curve) at 15 K under 395 nm excitation.

3.4. $GdVO_4$:1%Tb^{3+} and $LuVO_4$:1%Tb^{3+}

In figure 7 the 15 K excitation spectra of $GdVO_4$:Tb^{3+} and $LuVO_4$:Tb^{3+} are shown, monitoring the $^5D_4 \rightarrow {}^7F_5$ (548 nm) emission. They present the 250 and 320 nm bands of the VO_4^{3-} group, whereas the 376 nm band in $GdVO_4$:Tb^{3+} is assigned to the IVCT band of Tb^{3+}. The inset in figure 7 shows the temperature quenching behavior of this band.

Figure 8 presents the 15 K emission spectra of $GdVO_4$:Tb^{3+} and $LuVO_4$:Tb^{3+} during 370 nm excitation. The spectra show only $^5D_4 \rightarrow {}^7F_J$ multiplet emission lines. No

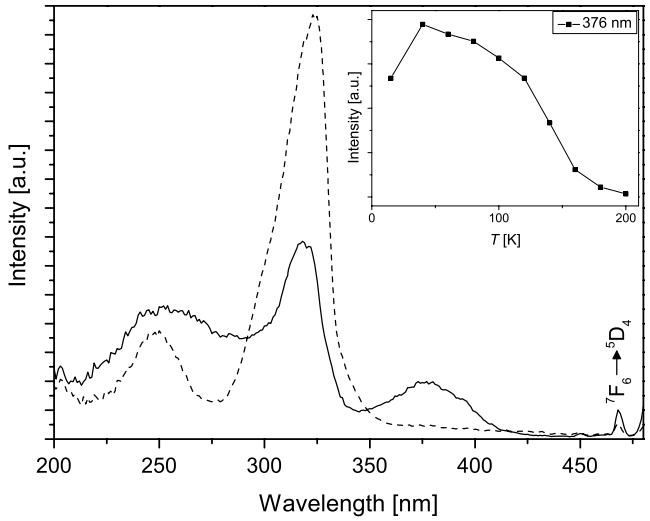

Figure 7. 15 K excitation spectra of $GdVO_4$:1%Tb^{3+} (solid line) and $LuVO_4$:1%Tb^{3+} (dashed line) monitoring the emission at 548 nm. The inset shows the temperature behavior of the $GdVO_4$:Tb^{3+} excitation band intensity at 376 nm.

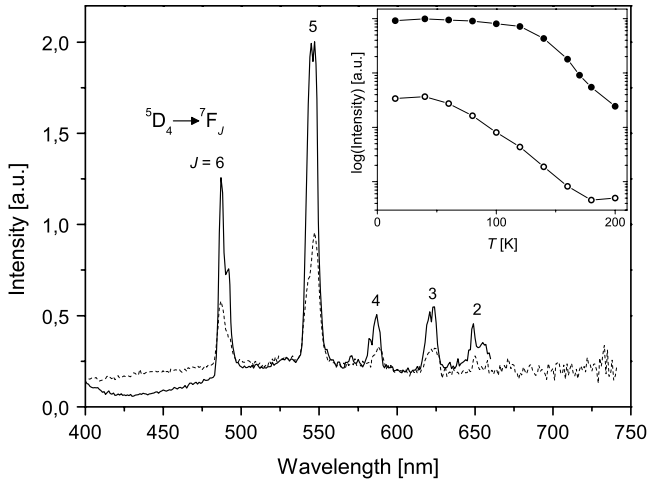

Figure 8. Emission spectra of $GdVO_4$:1%Tb^{3+} (solid line) and $LuVO_4$:1%Tb^{3+} (dashed line) recorded at 15 K under 370 nm excitation. The inset shows the temperature behavior of the peak intensity at 546 nm in $GdVO_4$:Tb^{3+} (upper curve, ●) and $LuVO_4$:Tb^{3+} (lower curve, ○) under 468 nm excitation; note that the intensity is displayed on a logarithmic scale.

emission from the Tb^{3+}:$^5D_3$ level can be seen. The inset of figure 8 shows the temperature quenching behavior of the $^5D_4 \rightarrow {}^7F_5$ (547 nm) emission under $^7F_6 \rightarrow {}^5D_4$ (468 nm) excitation both for $GdVO_4$:Tb^{3+} and $LuVO_4$:Tb^{3+}.

4. Discussion and conclusion

The excitation band at 320 nm (3.87 eV) in both $GdVO_4$ and $LuVO_4$ is taken as the first allowed VO_4^{3-} transition which defines the band gap energy. For the sake of convenience this band gap energy will be regarded in the following as the energy between the top of the VB and the bottom of the CB. Figure 9 illustrates the $Ln^{3+} \rightarrow V^{5+}$ IVCT transition both within

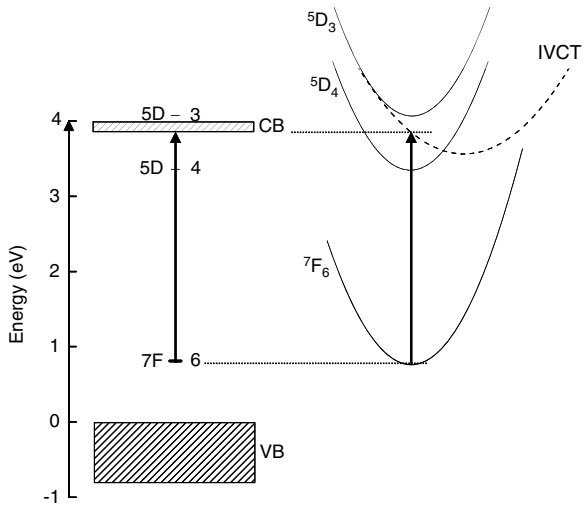

Figure 9. Energy level diagram (left side) and configurational coordinate diagram (right side) of $GdVO_4$:Tb^{3+}; arrows indicate the IVCT transition as used for energy level location.

the energy level diagram and the configurational coordinate diagram for $GdVO_4$:Tb^{3+}. According to this depiction the bottom of the CB as defined by us is somewhat higher in energy than the IVCT state relaxed to the equilibrium configuration in the configurational coordinate diagram (see figure 9).

4.1. Ln^{2+} 4f GS energy location

The location of the Ln^{2+} GS energies is usually found with the help of the Eu^{3+} CT band. This band is due to the transfer of an electron from an oxygen ligand to Eu^{3+}, thus forming Eu^{2+} in its ground state $4f^7$ level. In oxide compounds it is usually observed as a distinct broad excitation band with, depending on the type of compound, a maximum that may vary between 240 and 300 nm. From the energy $E^{CT}(Eu^{3+})$ of the Eu^{3+} CT band the CT energies of all other ions doped in the same compound can be derived via

$$E^{CT}(Ln^{3+}) \cong E^{CT}(Eu^{3+}) + \Delta E^{CT}(Ln^{3+}). \qquad (1)$$

The host independent constants $\Delta E^{CT}(Ln^{3+})$ are compiled in [3]. The Ln^{3+} CT energy gives information on the location of the 4f GS of the divalent ion relative to the top of the VB. In our measurements though we could not identify an O^{2-}–Eu^{3+} CT in $GdVO_4$:Eu^{3+} and $LuVO_4$:Eu^{3+}. Therefore, we have to assume that the 4f GS of Eu^{2+} is energetically located above the bottom of the CB for both types of compound.

4.2. Ln^{3+} 4f GS energy location

The method for locating the divalent lanthanide ground state energies is based on CT energy to the trivalent lanthanides. An analogous method is not applicable for locating the trivalent ground state energies because the Ln^{4+} valence is usually not stable in compounds. Another method was proposed by Dorenbos. The energy differences between the lowest 4f and lowest 5d states of both the divalent and the trivalent

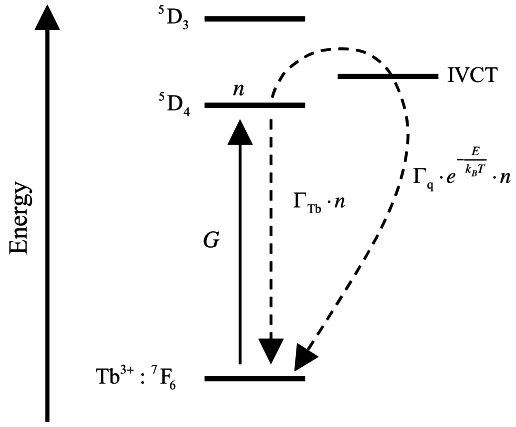

Figure 10. Energy level scheme illustrating the temperature quenching of Tb^{3+}:$^5D_4$ luminescence. The steady state condition for this first order reaction is fulfilled when $dn/dt = G - (\Gamma_{Tb} + \Gamma_q \cdot \exp(-E/k_B T)) \cdot n = 0$.

lanthanides are well known. Therefore, once the 4f ground state locations are known those for the lowest 5d states can also be located. It turns out that the absolute location of the lowest 5d state of divalent lanthanide ions relative to the host bands gradually changes when moving through the lanthanide series, but they never deviate more than 0.5 eV from each other. By assuming a similar constant energy for the lowest 5d states for the trivalent lanthanides, and by utilizing the known variation in 4f–5d energy differences with changing type of trivalent lanthanide ion, the 4f ground state energies of the trivalent lanthanides relative to the valence band can be found. An equation similar to equation (1) but with parameter values for the trivalent lanthanides was proposed. The proposed parameter values in [3] suggest that the Tb^{3+} ground state should be found 0.73 eV above the Pr^{3+} ground state. This would also imply that the IVCT band from Tb^{3+} to the CB should be at an energy 0.73 eV lower than that for Pr^{3+}. However, recently Boutinaud *et al* found about the same energy for the Pr^{3+} and the Tb^{3+} IVCT transitions in $LaVO_4$, $YNbO_4$ and $CaNb_2O_6$ [15]. The 0.06 eV difference between the maxima of the IVCT bands in $GdVO_4$:Pr^{3+} and $GdVO_4$:Tb^{3+} observed in this work confirms the findings of Boutinaud *et al*. Beside the IVCT energy, supporting evidence can be derived from the luminescence quenching of the Pr^{3+}:$^3P_0$ and Tb^{3+}:$^5D_4$ emission in order to place the 4f energy levels of Pr^{3+} and Tb^{3+} relative to the bottom of the CB. In the case of $GdVO_4$:Tb^{3+} an excitation at 370 nm shows $^5D_4 \rightarrow {}^7F_J$ multiplet emission but no emission from $^5D_3$ which is rather uncommon for low Tb doped compounds. This indicates that the Tb^{3+}:$^5D_3$ energy level is located energetically above the IVCT state in the configurational coordinate diagram which thus provides a non-radiative relaxation route for the $^5D_3$ electron (see figure 9). In $LuVO_4$:Tb^{3+} the same excitation also gave rise only to $^5D_4 \rightarrow {}^7F_J$ multiplet emission of Tb^{3+}. This shows that also in $LuVO_4$:Tb^{3+} the $^5D_3$ level must energetically be located above the IVCT state or the bottom of the CB. In order to derive the activation energies for the temperature quenching of the luminescence we assumed a simple model depicted in figure 10 using the example of Tb^{3+}. Within that model the temperature-dependent emission intensity is proportional to the steady state population, n, of the $^5D_4$ level:

$$I(T) \propto \Gamma_{Ln} \cdot n(T) = \frac{G}{1 + (\Gamma_0/\Gamma_{Ln}) \exp(-E/k_B T)}, \quad (2)$$

where G is the excitation rate to $^5D_4$, $\Gamma_0 \cdot \exp(-E/k_B T)$ is the rate constant for temperature-dependent and radiationless relaxation via the IVCT state, Γ_{Ln} is the rate constant for radiative transitions from the Ln^{3+} emitting level, E is the activation energy for temperature quenching of the $^5D_4$ luminescence and k_B is the Boltzmann constant. From equation (2) it follows that $I(T \rightarrow 0) \equiv I_0 \propto G$ is the luminescence intensity at low temperatures. The fitting parameters Γ_0/Γ_{Ln} and E for temperature quenching behavior of the Pr^{3+}:$^3P_0$ and Tb^{3+}:$^5D_4$ emission in AVO_4 (A = La, Gd, Lu) are shown in table 2. For $LaVO_4$ the parameters were derived from fitting data presented in [1]. From table 2 we see that the activation energy for temperature quenching of the Pr^{3+}:$^3P_0$ emission is about the same in $LaVO_4$:Pr^{3+} and $LuVO_4$:Pr^{3+} and very close to the activation energies of the Tb^{3+}:$^5D_4$ emission in both compounds. Apparently, the $^3P_0$ and $^5D_4$ levels are approximately at the same position in the band gap. As the Pr^{3+}:$^3H_4$–$^3P_0$ and the Tb^{3+}:$^7F_6$–$^5D_4$ energy differences just happen to be almost equally large, the Pr^{3+} and Tb^{3+} ground states should also be at the same position in the band gap. This is in agreement with the similarity of the Pr^{3+} and Tb^{3+} IVCT energies which has been identified by us in the excitation spectra. In the case of $GdVO_4$ the activation energies for temperature quenching of the Pr^{3+} and the Tb^{3+} emission are more than twice as large as the corresponding energies in $LaVO_4$ and $LuVO_4$ and also the PL intensities of $LuVO_4$:Ln^{3+} are about two times weaker than those of $GdVO_4$:Ln^{3+} (Ln = Pr, Tb; see figures 4 and 8). All spectra were recorded under similar conditions. This suggests that the Pr^{3+}:$^3P_0$ as well as the Tb^{3+}:$^5D_4$ energy level is energetically located even closer to the CB in $LaVO_4$ and $LuVO_4$ than in $GdVO_4$.

The Γ_0/Γ_{Ln} ratio of Tb^{3+} is always larger than that of Pr^{3+}. We attribute this to the fact that the lifetime of the Tb^{3+}:$^5D_4$ level is much longer than the lifetime of the Pr^{3+}:$^3P_0$ level in low doped compounds [19]. It can be seen that the Tb^{3+}:$^5D_4$ and the Pr^{3+}:$^3P_0$ levels, when placed by means of the activation energies given in table 2, are about 0.5 eV closer

Table 2. Rounded thermal quenching parameters Γ_0/Γ_{Ln} and E for emission spectra of $GdVO_4$:Tb^{3+} and $LuVO_4$:Tb^{3+}. The emission spectra were recorded under Tb^{3+}:$^7F_6 \rightarrow {}^5D_4$ and Pr^{3+}:$^3H_4 \rightarrow {}^3P_1$ excitation, respectively.

Sample	Emission band	Γ_0/Γ_{Ln} ($\times 10^3$)	E (meV)
$LaVO_4$:Pr^{3+}	$^3P_0 \rightarrow {}^3F_2$ (659 nm)	8	41
$LaVO_4$:Tb^{3+}	$^5D_4 \rightarrow {}^7F_5$ (546 nm)	57	19
$GdVO_4$:Pr^{3+}	$^3P_0 \rightarrow {}^3H_6$ (625 nm)	0.7	121
$GdVO_4$:Tb^{3+}	$^5D_4 \rightarrow {}^7F_5$ (546 nm)	17	114
$LuVO_4$:Pr^{3+}	$^3P_0 \rightarrow {}^3H_6$ (625 nm)	0.06	43
$LuVO_4$:Tb^{3+}	$^5D_4 \rightarrow {}^7F_5$ (547 nm)	0.3	37

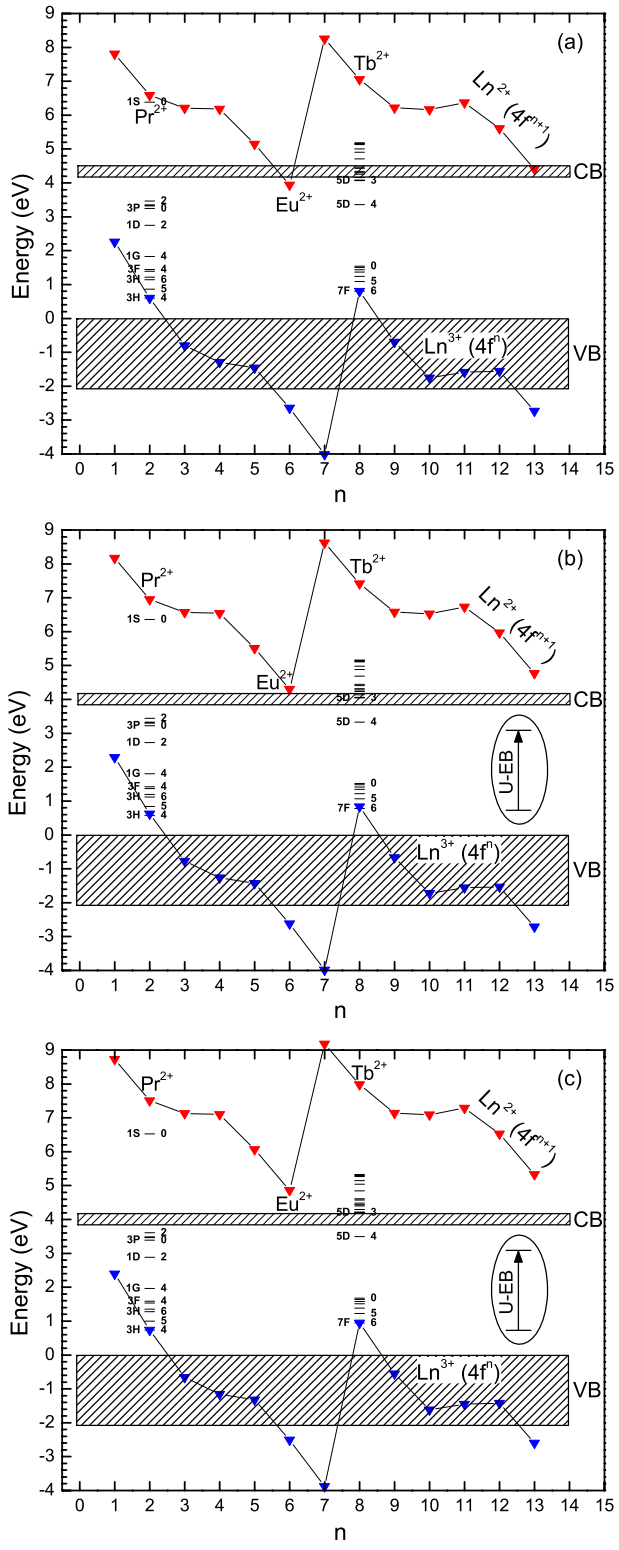

Figure 11. Energy level diagrams of $LaVO_4$:Ln^{3+} (a), $GdVO_4$:Ln^{3+} (b) and $LuVO_4$:Ln^{3+} (c). For Pr^{3+} and Tb^{3+} the 4f energy levels are also displayed. n = number of electrons in 4f shell of Ln^{3+}; U − EB = U excitation band as specified in text (it does not hold for all $GdVO_4$:Ln^{3+} and $LuVO_4$:Ln^{3+} materials).

to the bottom of the CB than when placed with the help of the IVCT energies. This difference can be understood in view of figure 9. We have chosen to use the IVCT transition energies as a foundation in order to place the Pr^{3+} and Tb^{3+} levels energetically in the energy gap. On this basis we can now predict the relative location of the 4f GS energies of all the other possible Ln^{3+} dopants in these orthovanadates by using the empirical model of Dorenbos. To account for the similar IVCT energies of Pr^{3+} and Tb^{3+} we have tilted the zig-zag curve of the trivalent Ln ions presented in earlier publications linearly with the difference in the ionic radii of Ln^{3+} and Ce^{3+} [20, 21]. The complete energy level diagrams are shown in figure 11. The energy level diagram of $LaVO_4$:Ln^{3+} which was presented in [1] differs from the one shown in figure 11 in two ways: (i) in [1] we assigned the band at 364 nm in the $LaVO_4$:Eu^{3+} excitation spectra to the Eu^{3+} CT. After a new analysis we would rather assign the shoulder in the excitation spectrum of $LaVO_4$:Eu^{3+} at about 315 nm to the Eu^{3+} CT. The revised position is taken into account in figure 11. (ii) Also the curve of the trivalent Ln ions has been rearranged in the diagram of $LaVO_4$. The activation energies shown in table 2 imply that also in the case of $LaVO_4$ the 4f ground states of Pr^{3+} and Tb^{3+} are located at similar energies. We have no clear evidence about the $Tb^{3+} \rightarrow V^{5+}$ IVCT energy in $LaVO_4$:Tb^{3+} but a weak excitation band can be seen in the excitation spectra of $LaVO_4$:Pr^{3+} at about 340 nm [1] or 347 nm [2]. The first value has been taken as a reference in figure 11.

Based on excitation spectra, we concluded that the lowest VO_4^{3-} transition is about 0.5 eV higher in energy in $LaVO_4$ than in $GdVO_4$ and $LuVO_4$. Even though $LaVO_4$ (space group $P2_1/n$, [22]) has a different crystal structure than $GdVO_4$ and $LuVO_4$ (space group $I4_1/amd$, [23, 24]), in all cases the vanadium ions are coordinated by four oxygen atoms with similar interatomic distances between V^{5+} and O^{2-} [5, 6, 22]. Blasse and Bril [11] reported on the dependence of the maximum of the vanadate emission band on the choice of A in compounds with formula AVO_4: the smaller the effective ionic radius of A with a certain coordination number, the more the maximum of the vanadate emission band is shifted to longer wavelengths. This can also be seen in the emission spectra of $LaVO_4$ [1], $GdVO_4$:Ce^{3+} and $LuVO_4$:Ce^{3+} (see section 3.1). None of the PL spectra shows 5d–4f emission or 4f–5d excitation. This indicates that in the three energy level diagrams presented in figure 11 the 5d states of the Ln dopant ions are located inside the CB. The diagrams of $GdVO_4$ and $LuVO_4$ also explain why no Tb^{3+}:$^5D_3$ emission could be observed in these orthovanadates as this state is energetically located inside the CB. The ground state energies of the divalent ions are all energetically located inside the CB as well, except for $LaVO_4$:Eu^{3+}, from which it follows that the orthovanadates, AVO_4, cannot contain Ln dopant ions with oxidation state (II). For the same reason these Ln dopant ions cannot even serve as metastable electron-traps. On the other hand the ground state energies of Ce^{3+}, Pr^{3+} and Tb^{3+} are energetically located above the VB and could therefore serve as stable hole-traps.

Acknowledgment

This work was supported by the Dutch Technology Foundation (STW).

References

[1] Krumpel A H, van der Kolk E, Dorenbos P, Boutinaud P, Cavalli E and Bettinelli M 2008 *Mater. Sci. Eng.* B **146** 114
[2] Boutinaud P, Mahiou R, Cavalli E and Bettinelli M 2005 *Chem. Phys. Lett.* **418** 181
[3] Dorenbos P 2003 *J. Phys.: Condens. Matter* **15** 8417
[4] Smith S H and Wanklyn B M 1974 *J. Cryst. Growth* **21** 23
[5] Mahapatra S and Rahmanan A 2005 *J. Alloys Compounds* **395** 149
[6] Chakoumakos B C, Abraham M M and Boatner L A 1994 *J. Solid State Chem.* **109** 197
[7] Wang X, Loa I, Syassen K, Hanfland M and Ferrand B 2004 *Phys. Rev.* B **70** 064109
[8] Blasse G and Bril A 1967 *Phil. Res. Rep.* **22** 481
[9] Shannon R D 1976 *Acta Crystallogr.* A **32** 751
[10] Ronde H and Blasse G 1978 *J. Inorg. Nucl. Chem.* **40** 215
[11] Blasse G and Bril A 1969 *J. Chem. Phys.* **50** 2974
[12] Boulon G 1971 *J. Physique* **32** 333
[13] Ryba-Romanowski W, Gołab S, Solarz P, Dominiak-Dzik G and Lukasiewicz P 2002 *Appl. Phys. Lett.* **80** 1183
[14] Schipper W J, Hoogendorp M F and Blasse G 1993 *J. Alloys Compounds* **202** 283
[15] Boutinaud P, Cavalli E and Bettinelli M 2007 *J. Phys.: Condens. Matter* **19** 386230
[16] Liu B, Shi C, Zhang Q and Chen Y 2002 *J. Alloys Compounds* **333** 215
[17] Brecher C, Samelson H, Lempicki A, Riley R and Peters T 1967 *Phys. Rev.* **155** 178
[18] Boutinaud P, Putaj P, Mahiou R, Cavalli E, Speghini A and Bettinelli M 2007 *Spect. Lett.* **40** 209
[19] Yen W M, Shionoya S and Yamamoto H (ed) 2007 *Phosphor Handbook* 2nd edn (Boca Raton, FL: CRC Press) ISBN 0-8493-3564-7
[20] Thiel C W, Gruguel H, Wu H, Sun Y, Lapeyre G J, Cone R L, Equall R W and Macfarlane R M 2001 *Phys. Rev.* B **64** 085107
[21] Thiel C W, Gruguel H, Sun Y, Lapeyre G J, Macfarlane R M, Equall R W and Cone R L 2001 *J. Lumin.* **94** 1
[22] Rice C E and Robinson W R 1976 *Acta Crystallogr.* B **32** 2232
[23] Mahapatra S and Ramanan A 2005 *J. Alloys Compounds* **395** 149
[24] Chakoumakos B C, Abraham M M and Boatner L A 1994 *J. Solid State Chem.* **109** 197